International Journal of Fluid Machinery and Systems
Vol. 12, No. 4, October-December 2019
DOI: http://dx.doi.org/10.5293/IJFMS.2019.12.4.388
ISSN (Online): 1882-9554

Original Paper

Detailed Analysis of Flow in Two Pelton Turbines with Efficiency and Cavitation Prediction

Dragica Jošt[1], Aljaž Škerlavaj[1], Valentin Pirnat[1], Mitja Morgut[2] and Enrico Nobile[2]

[1]Kolektor Turboinštitut, Rovšnikova 7, 1210 Ljubljana, Slovenia,
dragica.jost@kolektor.com, aljaz.skerlavaj@kolektor.com, valentin.pirnat@kolektor.com
[2]University of Trieste, Italy, mmorgut@units.it, nobile@units.si

Abstract

This paper presents results of the numerical analysis of two Pelton turbines: a 6-jet turbine for middle head and a 2-jet turbine for high head. For the 6-jet turbine losses in manifold, quality of the jets and turbine efficiency were predicted and validated with the experimental data. Additional improvement of accuracy of efficiency prediction was obtained with cavitation modelling. It was also checked that there was no interaction between the evacuating water sheets and the incoming jets. For a 2-jet turbine cavitation prediction was done. Small vapour cavity at the inner side and a larger one at the back side of the bucket were observed. Detailed analysis of cavitation and condensation processes showed that the conditions for cavitation pitting were not fulfilled.

Keywords: Pelton turbine, multiphase flow, free surface modelling, cavitation, efficiency prediction.

1. Introduction

Compared to Kaplan and Francis turbines, complete CFD analysis of Pelton turbines is, because of the complex two phase flow, far more difficult and more time consuming. For this reason the first useful results were obtained relatively late. In 2002 Parkinson et al. [1] described a water jet from a Pelton turbine injector on the basis of experimental and numerical results. One of the first attempts to calculate free surface flow in a rotating bucket was done by Kvinsky et al. [2]. A bucket flow simulation using three adjacent buckets with efficiency prediction was illustrated by Mack and Moser [3]. Perrig [4] investigated flow in buckets by unsteady onboard wall pressure measurements, high-speed onboard and external flow visualizations, water film thickness measurements and CFD simulations. Efficiency prediction for a 2-jet Pelton turbine at different operating regimes was presented by Jošt at al. [5]. The effect of grid refinement and the importance of accurate description of real jet prescribed at the runner inlet, instead of the theoretical one, was emphasized. A great step forward was done by Santolin et al. [6]. They performed the simulation of an entire single-jet Pelton turbine. The runner was coupled with the final part of the penstock and the needle nozzle. The negative effect of the real jet, perturbed by the needle wake and secondary flows, in comparison with an ideal theoretical jet, was presented. In an attempt to overcome the mesh difficulties of the VOF method, the analysis by Marongiu et al. [7] was performed with a particle-based method. Its main drawback was a significant increase of computational time. A new approach was presented by Vessaz et al. [8]. They validated Finite Volume Particle Method (FVPM) and showed that it was an accurate tool to capture the deviation of high-speed water jets by rotating Pelton buckets. With increasing number of particles the accuracy of results was improved, so the method proved to be stable and consistent. The disadvantage of the method is, again, a long computing time. In addition, the discrepancy between calculated and measured values of torque was significant. Regarding the cavitation prediction an important achievement was reported by Rossetti at al. [9]. They presented a simulation of cavitating flow in a Pelton runner and suggested a practical criterion for risk assessment of cavitation pitting. In [10] the numerical analysis for two Pelton turbines was presented. For the 6-jet turbine the quality of the jets and possibility of interaction between the evacuating water sheets and the jets were checked. Predicted efficiency for maximal opening was compared to the experimental value. For the 2-jet turbine a numerical simulation of cavitating flow in the runner was presented.

This paper is an extension of the previous work of Jošt et al. [10]. New transient results in manifold obtained on refined meshes are added. A detailed analysis of unsteady flow in the runner and variation of torque due to rotation of the observed bucket are presented. Torque on the shaft obtained with and without cavitation modelling is presented with the aim to see the potential of cavitation modelling for improving the accuracy of predicted efficiency. In the second part, where a numerical simulation of cavitating flow in the runner of a high head 2-jet Pelton turbine is presented, a detailed illustration of formation and decay of vapour cavities is added. A careful inspection of the results has been done in order to check whether the conditions for cavitation pitting are fulfilled and

Received March 28 2019; accepted for publication December 1 2019: Review conducted by Yoshinobu Tsujimoto. (Paper number O19058S)
Corresponding author: Dragica Jošt, Senior researcher, dragica.jost@kolektor.com

* Part of this paper was presented at the 29th IAHR Symposium on Hydraulic Machinery and Systems, held at Kyoto, Sept. 16-21st, 2018.

subsequent erosion can be expected.

2. Mathematical model

In the homogeneous multiphase transport equation-based model, the cavitating flow can be described by the following set of governing equations:

$$\begin{cases} \nabla \cdot \boldsymbol{U} = \dot{m}\left(\frac{1}{\rho_l} - \frac{1}{\rho_v}\right) \\ \frac{\partial(\rho \boldsymbol{U})}{\partial t} + \nabla \cdot (\rho \boldsymbol{U}\boldsymbol{U}) = -\nabla P + \nabla \cdot \boldsymbol{\tau} + S_M \\ \frac{\partial \gamma}{\partial t} + \nabla \cdot (\gamma \boldsymbol{U}) = \frac{\dot{m}}{\rho_l} \end{cases} \quad (1)$$

The cavitating flow is modelled as a mixture of two species i.e. vapour and liquid behaving as one. Both phases are considered incompressible. They share the same velocity $\boldsymbol{U}$ and pressure fields P. The mixture density, ρ, and dynamic viscosity, μ, are scaled, respectively, as:

$$\begin{aligned} \rho &= \gamma\rho_l + (1-\gamma)\rho_v \\ \mu &= \gamma\mu_l + (1-\gamma)\mu_v \end{aligned} \quad (2)$$

The interface mass transfer rate due to cavitation, $\dot{m}$, can be modelled using different mass transfer models available in literature. In this study the mass transfer model proposed by Zwart et al. [11] was used:

$$\dot{m} = \begin{cases} -F_e \frac{3 r_{nuc}(1-\alpha)\rho_v}{R_B}\sqrt{\frac{2}{3}\frac{P_v - P}{\rho_l}} & if\ P < P_v \\ F_c \frac{3\alpha\rho_v}{R_B}\sqrt{\frac{2}{3}\frac{P - P_v}{\rho_l}} & if\ P < P_v \end{cases} \quad (3)$$

The mass transfer rate was considered positive if directed from vapour to liquid phase and the maximum density ratio, ρ_l/ρ_v, was clipped to 1000 as in [12] for solver stability reasons. In order to model turbulence effects different approaches can be applied, mainly, depending on the required accuracy and the available computational resources. In this study we adopted the standard RANS approach in combination with the SST turbulence model, and the more advanced SAS-SST model available in CFX. For a detailed description of the considered models we refer to [13-15]. The SAS-SST model is an improved unsteady-RANS formulation, with the ability to adapt the length scale to resolved turbulent structures by including the von Karman length-scale into the turbulence scale equation. The information given by the von Karman length scale allows the SAS-SST model to dynamically adjust to resolved structures mimicking a LES-like behaviour in unsteady regions of the flow field. At the same time, the model provides standard RANS capabilities in stable flow regions.

3. Numerical set-up and computational meshes

The numerical simulations were performed with ANSYS CFX, Release 15.5 and Release 18.2. As pointed out in the former section, turbulence was modelled with the k-ω SST model, only for transient simulations in manifold besides the SST also the SAS SST model was used. The advection term was discretized with the high resolution scheme (HRS) implemented in ANSYS CFX code. For time discretization the second order Euler scheme was used.

Due to the high complexity of the geometry, a combination of structured and unstructured meshes was used. Before mesh generation, the theoretical thickness of the jets was calculated and an initial mesh refinement was done in regions where interface between water and air was expected. Basic mesh for manifold with injectors and jets consisted of 14.2 million elements with 12.6 million nodes. Additional refinement was done with automatic grid refinement in regions where the interface between water and air was obtained on the basic mesh. This refinement was done in separate flow simulation in one injector. Refined mesh was used for all six injectors and jets together with the manifold. After the refinement the mesh consisted of 31.9 million elements with 20.4 million nodes (Fig. 1(a) and Fig. 1(b)). Details of the manifold on the mid cross-section after mesh refinement for servomotor located inside and outside the nozzle are presented in Fig. 1(c). For runner analysis the computational domain was reduced to one half due to the symmetry. The unstructured grid consisted of about 46 million elements with 21 million nodes. The mesh can be seen in Fig. 2.

For cavitation prediction the problem was reduced, to maintain the computational costs within acceptable limits, to five runner buckets and one jet. The unstructured mesh was rather coarse in the regions without buckets and significantly refined on the buckets, especially at the regions where cavitation was expected (see Fig. 3). The mesh consisted of 10.75 million elements with 4.4 million nodes.

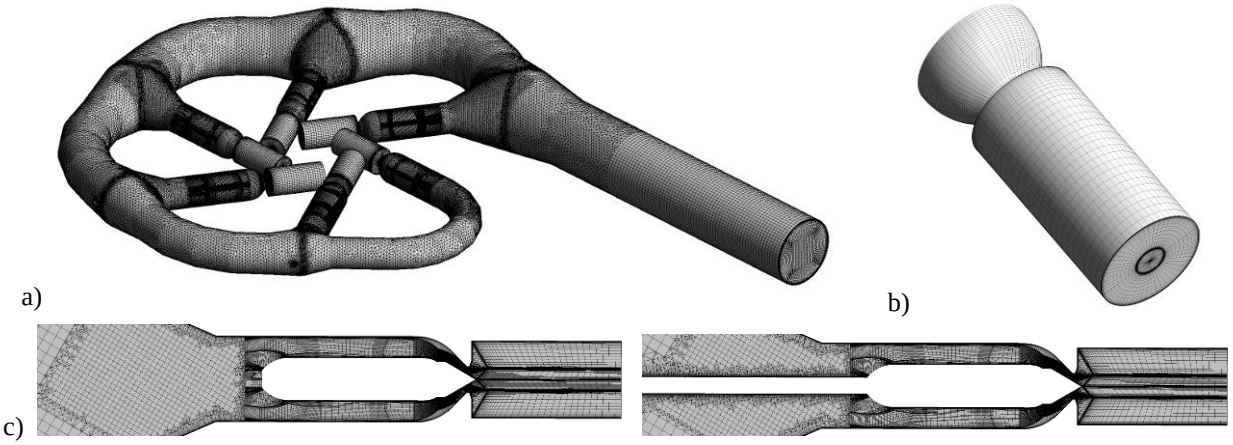

Fig. 1 Computational domain and mesh for flow analysis in the manifold with injectors and jets. a) complete mesh, b) sub-domain for automatic mesh refinement, c) detail of the meshes on mid cross-section for servomotors inside the nozzles (left) and for servomotors outside the nozzles (right).

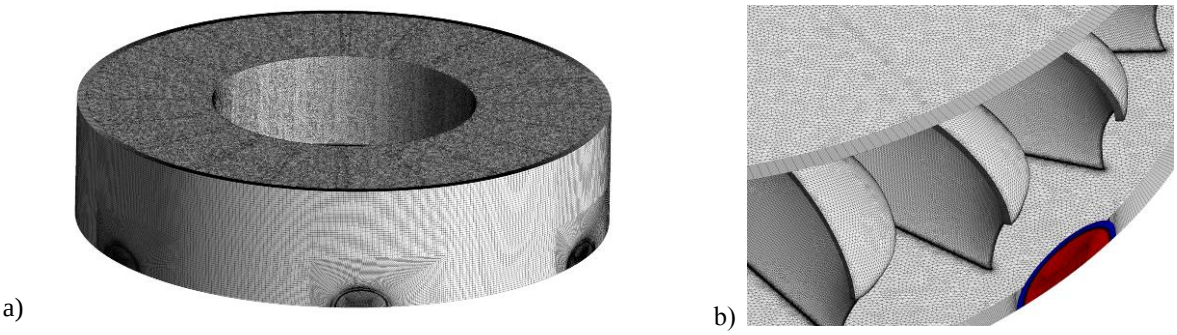

Fig. 2 Computational domain and mesh for runner analysis. a) complete mesh, b) detail

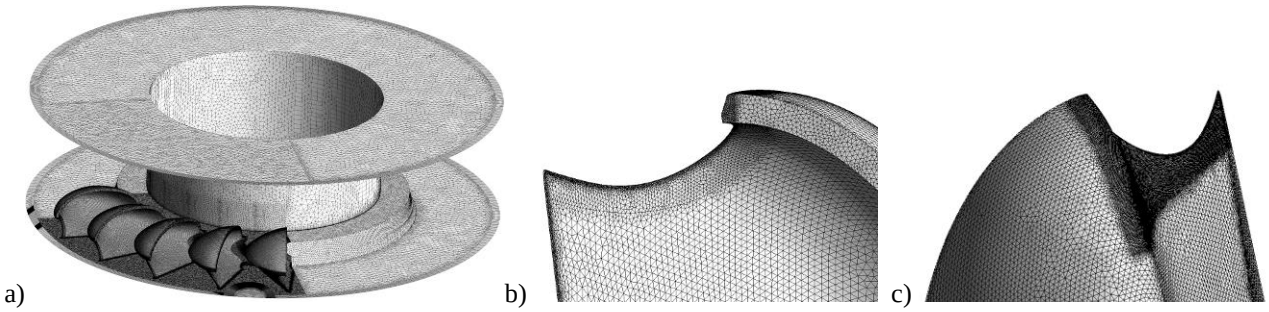

Fig. 3 Computational mesh for cavitation prediction in a high-head Pelton turbine. a) mesh, b) mesh refinement at the inner side of the bucket, c) mesh refinement at the back side of the bucket

4. Numerical flow simulation in a 6-jet Pelton turbine

The analysis was divided into three parts. At first, the analysis of the flow in the manifold with jets was performed. Secondly, the interaction between jets and buckets in the runner was investigated. Simulations were done for the model and for the prototype. In the third part, analysis with cavitation modelling was done for 1-nozzle operation, prototype size, to see the effect of cavitation modelling on accuracy of the efficiency prediction.

4.1 Flow in the manifold with injectors and jets

The proper design of manifold with injectors is extremely important for good performance of Pelton turbines. Discharge should be equally distributed between all injectors and flow energy losses should not exceed 2% of the head. Even more important is the quality of the jets. Secondary velocities caused by bends in the manifold are highly undesirable because they can cause jet dispersion and deviation [16].

In this study a steady state analysis of the flow in the manifold with six injectors was performed with the following boundary conditions: flow rate at the inlet of the manifold, outflow with averaged static pressure at the end surfaces of the cylinders behind the nozzles (see Fig. 1) and opening with static pressure and air as a fluid (Air Volume Fraction = 1) on cylindrical surfaces.

For the model, contrary to the prototype, servomotors, which enable to change the opening by moving the needle, were located outside the manifold. The needle rods, which connect the needles with the servomotors, pass through the manifold and slightly

influence the flow. To check the effect of this difference between the model and the prototype (see Fig. 1(c)), flow in the manifold was analysed for both options.

The simulations were performed for the model and for the prototype size. Analysis of the flow in the manifold was done for three needle strokes. For maximal opening additional steady state and transient simulations were performed on refined grid. Besides flow energy losses in the manifold the quality of the jets was analysed. With this objective, the shape of the jets was checked and secondary velocities in the jets were calculated. Manifold was analysed also for 1-nozzle operation. Analysis of flow in manifold for the prototype size was done mostly to get inlet conditions for runner flow simulation and it was performed only for the maximal opening.

Numerical results showed that flow rate is equally distributed between the injectors. For the smallest opening the deviation from equal distribution was less than 0.1%, while for the optimal and maximal opening the deviation was less than 0.02%.

Relative flow energy losses are presented in table 1. It can be seen that in case of servomotors outside the manifold the losses are slightly higher than when the servomotors are inside the manifold. The losses are larger for small openings. The effect of mesh refinement on losses was very small and in addition, with transient simulations nearly the same values of losses were obtained. Losses for the prototype size are relatively smaller than those for the model.

Table 1 Flow energy losses in manifold, 6-nozzle operation

Configuration	Size	$A_0/A_{0,BEP}$	Grid density	Simulation type	Losses $\Delta H/H$ *100 (%)
Servomotor outside manifold	model	0.47	basic	steady state	1.94
Servomotor outside manifold	model	1	basic	steady state	1.27
Servomotor outside manifold	model	1.83	basic	steady state	1.23
Servomotor outside manifold	model	1.83	refined	steady state	1.20
Servomotor outside manifold	model	1.83	refined	transient, SST	1.20
Servomotor outside manifold	model	1.83	refined	transient, SAS SST	1.21
Servomotor inside nozzle	model	0.47	basic	steady state	1.89
Servomotor inside nozzle	model	1	basic	steady state	1.25
Servomotor inside nozzle	model	1.83	basic	steady state	1.16
Servomotor inside nozzle	model	1.83	refined	steady state	1.17
Servomotor inside nozzle	model	1.83	refined	transient, SST	1.15
Servomotor inside nozzle	prototype	1.83	refined	steady state	0.84

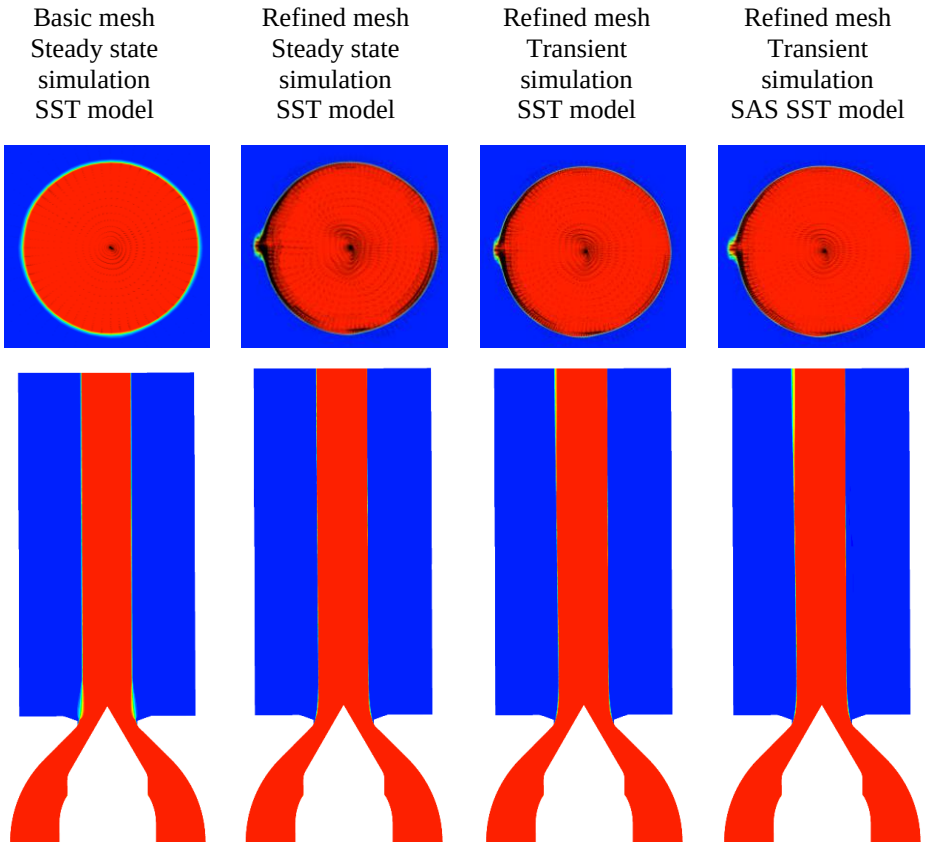

Fig. 4 Shape of the jet presented with Contours of Water Volume Fraction and vectors of secondary velocities on cross-section of the jet behind the nozzle 4 (red – water, blue –air), 6-nozzle operation.

The quality of the jets was checked by observation of the jet shape (see Fig. 4) and by calculation of secondary velocities at the jet cross-section. In order to calculate secondary velocity for each injector local coordinate systems were defined in such a way that the z axis corresponds to the needle axis. Secondary velocity V_{sec} was then defined with the expression $V_{sec} = \sqrt{V_x^2 + V_y^2}$.

The effect of grid refinement on the shape of the jet cross section and on the secondary velocity can be seen in Fig. 4. On the basic mesh the cross section of the jet is nearly a perfect circle and secondary velocity is small. With grid refinement small perturbation of the jet due to the bend of the manifold can be observed and secondary velocity increases. With transient simulation performed on the refined grid no significant difference in comparison to the steady state results on the same grid was obtained. The results are presented for the jet behind the nozzle 4, where secondary velocity is the largest. The nozzles are numbered in the direction of the flow.

In table 2 results for 1-nozzle operation, model size, maximal opening ($A_0/A_{0,BEP}$ = 1.83) are presented. As expected, flow energy losses in the manifold are the largest when the nozzle 6 is active. At the same time, for the nozzle 6 being active, the measured efficiency is the highest. This can be explained with the effect of secondary velocity in the jets on turbine performance. For 1-nozzle operation secondary velocity is the largest in the jet behind the nozzle 4. For nozzles 1, 2, 3, 4 and 6 negative correlation between secondary velocity and measured turbine efficiency can be clearly seen. An exception is nozzle 5, where measured efficiency was the smallest in spite of relatively small secondary velocity. 1-nozzle operation was numerically analysed also for the best efficiency point and the same negative correlation between secondary velocity and efficiency was observed, exception was again the nozzle 5. Therefore it can be suspected that on the test rig the nozzle 5 was not accurately positioned. Nevertheless, from the results in table 2 it can be concluded, that for high turbine efficiency the quality of the jets is even more important than flow energy losses in the manifold.

The results (velocity and thickness of the jets) of steady state simulations on refined mesh for model and prototype size were used as inlet boundary conditions for transient simulations in the runner.

Table 2 Results for 1-nozzle operation, model size, $A_0/A_{0,BEP}$ =1.83
Relative flow energy losses in the manifold, averaged relative secondary velocity and difference in measured efficiency for different nozzle being active. Nozzles are numbered in the flow direction.

Active nozzle	$\Delta H/H$ *100 (%)	v_{sec}/v *100 (%)	$\Delta\eta=\eta_i-\eta_6$ (%)
1	0.81	0.097	-0.06
2	0.84	0.077	-0.01
3	0.90	0.153	-0.24
4	0.92	0.195	-0.27
5	0.91	0.100	-0.38
6	0.99	0.074	0.00

4.2 Interaction between jets, buckets and evacuating water sheets in the runner and prediction of turbine efficiency

A computational domain for runner analysis consisted of two parts: a rotating part that comprises the runner and a stationary thin ring with six inlets (see Fig. 5(a)) where distribution of water and air and velocity components are prescribed. The other boundary conditions are presented in Fig. 5(b). The time step corresponded to 0.25 degrees of runner rotation.

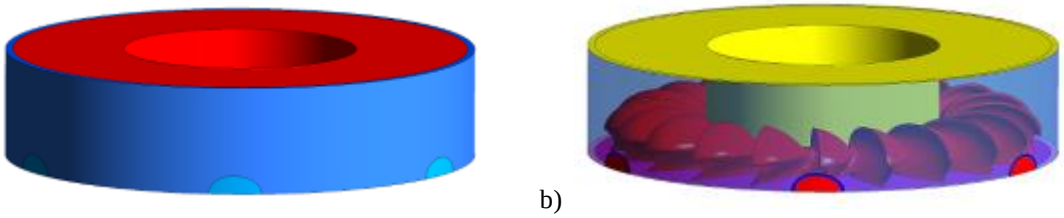

a) b)

Fig. 5 Computational domain and boundary conditions.
a) rotating part (red) and stationary part with six inlet regions (blue);
b) boundary conditions: walls - red, opening - yellow, symmetry - magenta, outlet - transparent blue, inlets are coloured with Water Volume Fraction

The results of the simulation are velocity and pressure distribution in the whole domain, as well as the shape of the jets and evacuating water sheets and an interaction between them (see Fig. 6).

From pressure distribution on the runner buckets, the torque on the shaft was calculated. At the beginning of the simulation the whole domain is filled with air and torque on the shaft is zero. During the simulation the jets get closer to the runner and when they impact the buckets the torque starts to rise. After approximately 200 time steps the value of the torque stabilizes (see Fig. 7), only periodic oscillation remains. For calculation of efficiency the averaged value of torque during the last 36 deg. of runner revolution was used. In Fig. 6(a) regions with very low absolute pressure can be observed. In fact, values presented with dark blue are lower than the vapour pressure, because cavitation was not modelled. This inaccuracy in pressure affects the calculated torque on the shaft and, consequently, the values of predicted efficiency.

Numerical results for the model were compared to the experimental values obtained on the test rig (see Fig. 8). The flow rate was input data, therefore its numerical and experimental values are the same. Numerical values of head, torque and efficiency are lower than the experimental ones. The largest discrepancy is for the value of torque, where the calculated value is 3.51% smaller than the measured one. Efficiency was calculated also for the prototype size, the value was 0.11% higher than that for the model.

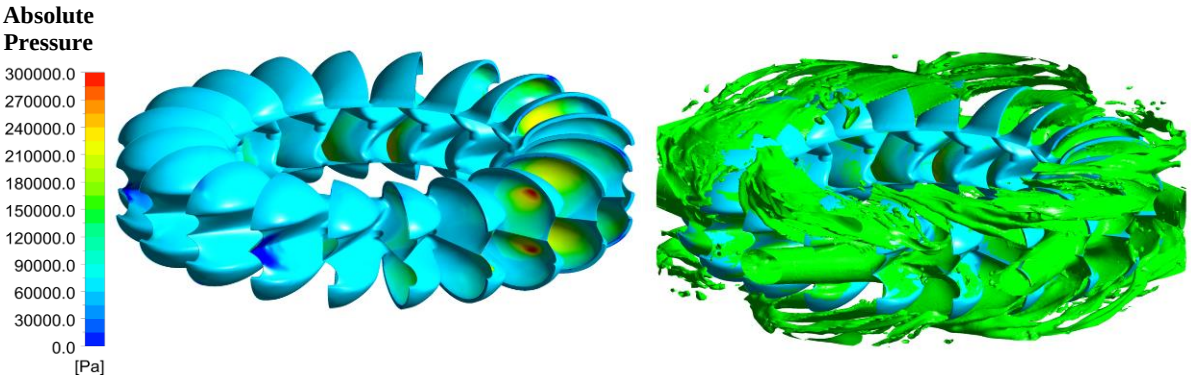

Fig. 6 Pressure distribution on the buckets (left) and water jets and evacuating water sheets presented as iso-surface of Water Volume Fraction = 0.5 (right), 6-nozzle operation, model size.

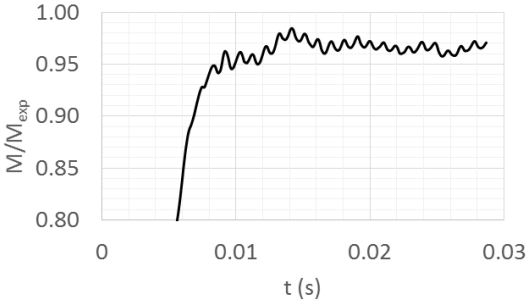

Fig. 7 Torque on the shaft during the simulation, model size, 6-nozzle operation, $A_0/A_{0,BEP}$ = 1.83.

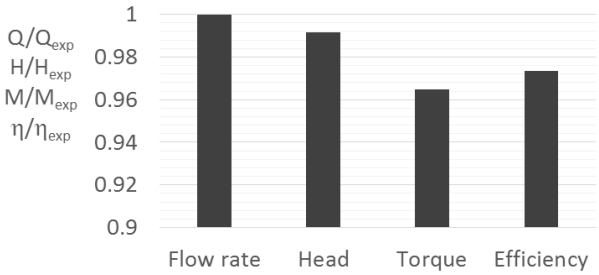

Fig. 8 Comparison of numerical results to the experimental values, model size, 6-nozzle operation, $A_0/A_{0,BEP}$ = 1.83.

For the prototype two simulations of flow in the runner were performed: one with single-nozzle operation and the other for 6-nozzle operation, both for $A_0/A_{0,BEP}$ = 1.83. For 1-nozzle operation detailed analysis of flow conditions around one bucket was done. The analysis starts at the moment, when the jet impacts the observed bucket, which starts to contribute to the torque on the shaft, and ends at the moment when the last portion of water lefts the same bucket and its contribution is equal to zero again. The results for six positions of the chosen bucket regarding the jet are presented in Fig. 9. In the first column the contribution of the observed bucket to the torque during the complete cycle is presented. The contribution at the moment of observation is marked with a black triangle. Jets and evacuating water sheets in the second and the third columns are presented as iso-surfaces with 50% of water (Water Volume Fraction = 0.5). In the fourth and the fifth columns pressure distribution on the inner and the back sides of the bucket is depicted.

At the first position the jet impacts the back side of the cut out lips, where pressure consequently increases. Pressure on the inner side is uniform because the inner side of the bucket is not in contact with the jet yet. At this moment the contribution of the observed bucket to the torque on the shaft is slightly negative. At the second position the jet impacts the upper inner side of the bucket where pressure increases. At the back side of the bucket there is quite a large region with pressure lower than vapour pressure (cavitation is not modelled!). Due to this unrealistic low pressure at the back side the contribution of the bucket to the complete torque on the shaft is a bit overestimated. At the position 3 the whole jet is feeding the bucket, but still a relatively small part of the bucket is in contact with water. On the back side only a small region with low pressure remains. The contribution of the bucket to the complete torque is increasing. At the position 4 the jet is already feeding the next bucket, but nearly the whole inner side of the observed bucket is still filled with water and pressure is high. The contribution of the observed bucket to the torque is maximal. After this moment the water starts to leave the bucket and therefore the contribution of the observed bucket to the torque starts to decrease. At position 5 the water is leaving the bucket. Pressure is higher only at outer part of the inner side, while at the back side it is uniform. The contribution of the bucket to the torque is considerably smaller than at the previous position. At position 6 the last portion of water is leaving the bucket and the contribution to the torque is close to zero.

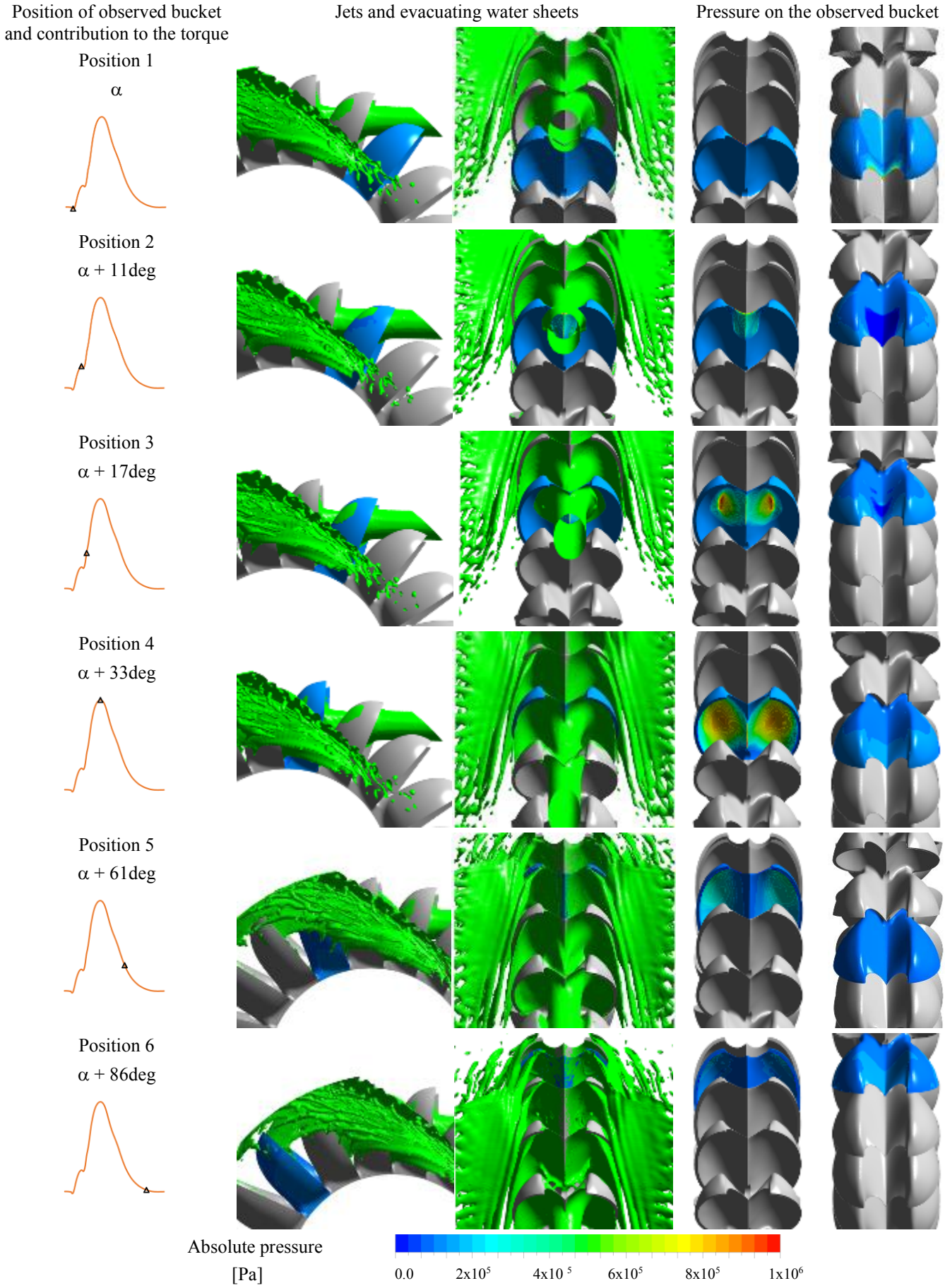

Fig. 9 Jets, evacuating water sheets and pressure distribution on the inner and on the buck sides of the observed bucket during one cycle, prototype size, 1-nozzle operation.

Special attention was paid to check possible interaction between the evacuating water sheets and the jets for 6-nozzle operation, prototype size. The results at several time steps were carefully analysed. In Fig. 10 iso-surfaces with 30% of water (Water Volume Fraction = 0.3) are presented for two time steps. With Water Volume Fraction = 0.3 instead of 0.5 a bit thicker jets and evacuating water sheets are obtained. So the possibility of interaction between them is larger and we are on the safe side. On the left part of the pictures the iso-surfaces are coloured by water velocity, while on the right part they are coloured by wall distance. Discontinuity in colour shows that there is a gap between the jet and the evacuating water. So there is no interaction between the evacuating water sheets and the approaching jet, although the bucket is never empty. In Fig. 11 it can be seen that evacuating water sheets do not impact the previous buckets.

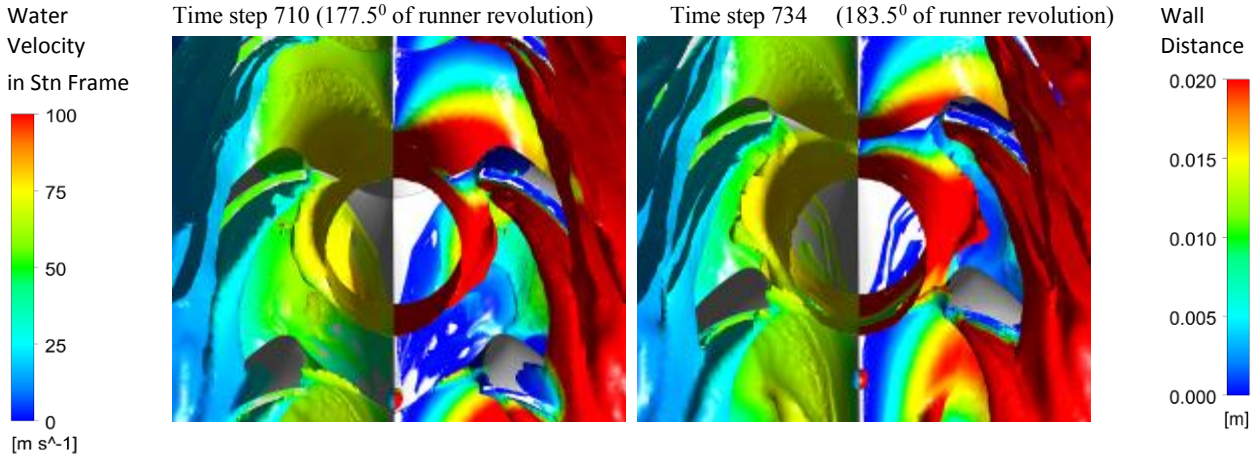

Fig. 10 Water jets and evacuating water sheets presented by iso-surface of Water Volume Fraction = 0.3. Left half is coloured by water velocity, while the right half of the pictures is coloured by wall distance.

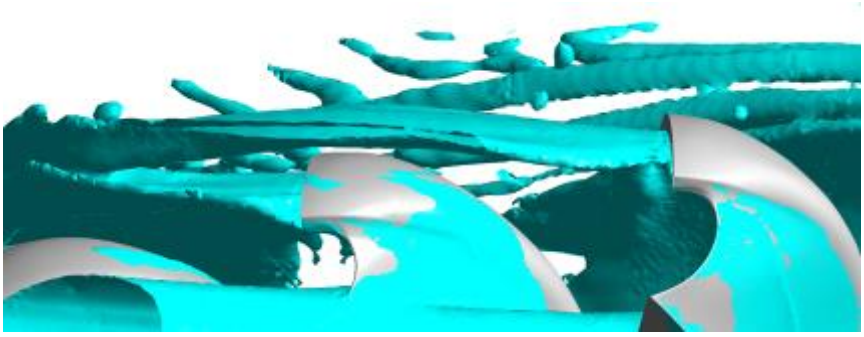

Fig. 11 Iso-surface of Water Volume Fraction = 0.3. Prototype size, 6-nozzle operation.

A contribution of one bucket to the complete torque on the shaft for 1-nozzle and 6-nozzle operation is presented in Fig. 12. For 1-nozzle operation the bucket contributes to the torque during approximately 90 degrees of runner revolution. For 6-nozzle operation before all the water leaves the bucket the next jet impacts it. Therefore during 6-nozzle operation at each moment all the buckets contribute to the torque (see Fig. 13). The runner consists of 20 buckets and there are 6 jets, therefore $M_i = M_{i+10}$, where M_i is the contribution of bucket #i to the torque.

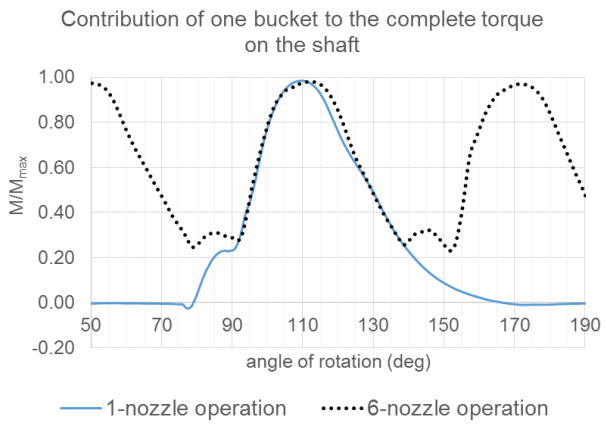

Fig. 12 Contribution of one bucket to the torque, prototype size, 1-nozzle and 6-nozzle operation.

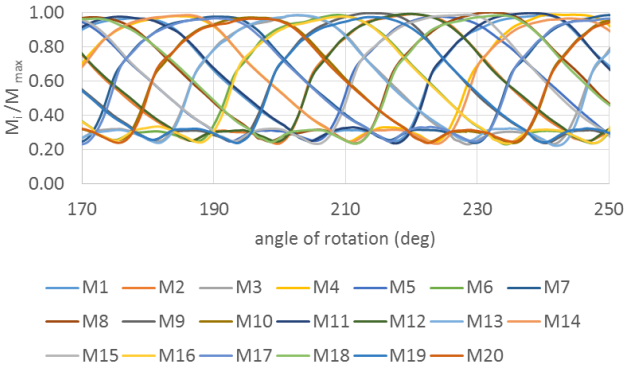

Fig. 13 Contributions of all buckets to the torque on the shaft, prototype size, 6-nozzle operation.

4.3 Effect of cavitation modelling on predicted efficiency

Prediction of cavitation in a Pelton turbine is very time consuming. Three-component flow consisting of water, water vapour and air has to be modelled. Furthermore, double precision of calculation has to be used, in order to improve the accuracy of the results and to avoid sudden overflows due to accumulation of numerical errors. Even without cavitation the simulation for the prototype size for 6-nozzle operation was very unstable. For these reasons the simulation with cavitation modelling was done only for the 1-nozzle operation.

The simulation started from the results with no cavitation modelling. Time step corresponded to 0.1 deg. of runner revolution. For this configuration (all buckets), the results are too large to be stored and checked after each time step. Therefore only selected variables were stored after each 40 iterations and detailed analysis of formation and decay of vapour cavities was not performed. The study in this section is focused on the effect of cavitation modelling on the predicted torque on the shaft and efficiency.

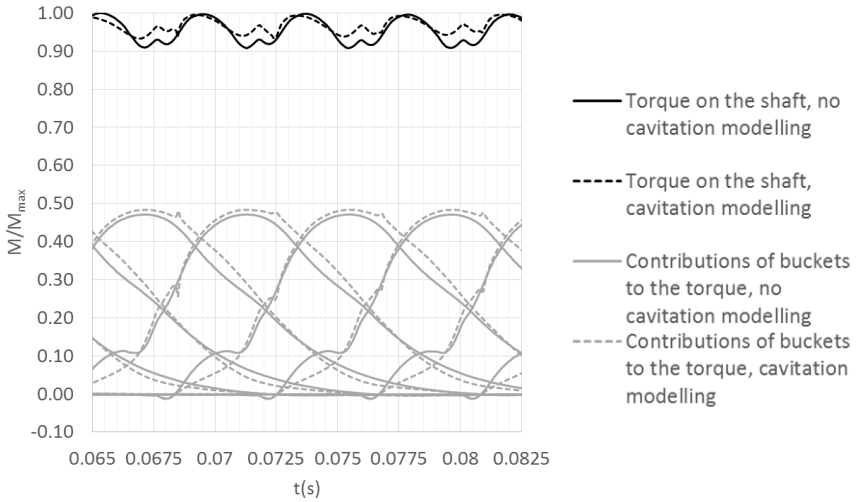

Fig. 14 Complete torque and contributions of eight successive buckets. Comparison of results without and with cavitation modelling, 1-nozzle operation, prototype size

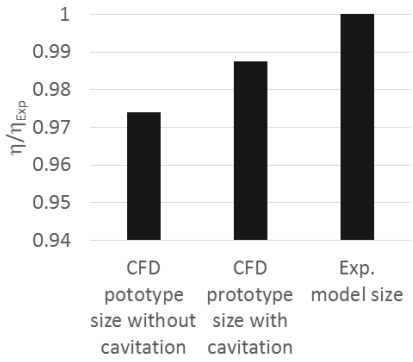

Fig. 15 Predicted and measured efficiency, 1-nozzle operation

During the simulation contributions of all buckets to the torque on the shaft and the complete torque were monitored. In Fig. 14 a comparison of torque values obtained with and without cavitation modelling is presented. With cavitation modelling an unreal, negative pressure is replaced with vapour pressure. Therefore in case of cavitation at the back side of the bucket its contribution to the torque on the shaft decreases, while when cavitation appears at the inner side of the bucket larger torque is obtained. At each moment five successive buckets contribute to the complete torque. In Fig. 14 it can be seen that with and without cavitation modelling approximately the same peak values of torque were obtained, while minimal and averaged values are smaller when cavitation was not modelled. For efficiency calculation averaged values during the last 54 deg. (three periods) of runner rotation were used. Comparison of predicted efficiency with the experimental values for the model size can be seen in Fig. 15. With cavitation modelling 1.35% higher efficiency was obtained and the agreement with the laboratory measurements was improved.

5. Cavitation prediction for a 2-jet high head Pelton turbine

Cavitation prediction was done for a prototype of a 2-jet high head Pelton turbine with runner diameter D = 1.2 m. The runner consists of 20 buckets.

In this case the simulation was reduced to five runner buckets (see Fig 16). Due to the symmetry the computational domain was reduced to one half. At the inlet the velocity and thickness of the jet obtained in a previous numerical analysis of the flow in manifold with injectors and jets (as in section 3.1) were prescribed. Computational mesh was significantly refined in regions where cavitation was expected (see Fig. 3(b) and Fig. 3(c)).

At the beginning of the simulation the whole computational domain was filled with air. It took some time before the jet impacted the first bucket, therefore the first 36 degrees of runner rotation were performed without cavitation modelling. For this part of the simulation the time step was equal to the time needed for 0.5 deg. of runner revolution. After the 36 deg. of runner revolution the cavitation was included. Time step was reduced to 0.1 deg. of runner revolution and additional 360 time steps were performed.

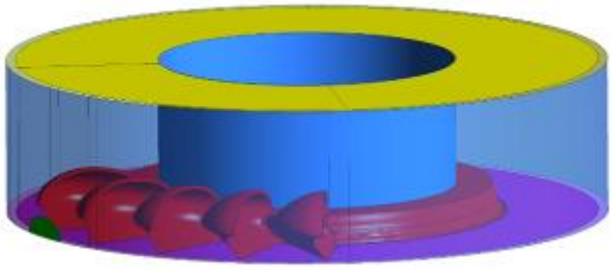

Fig. 16 Computational domain for cavitation prediction. The position of the buckets at the beginning of the simulation. magenta – symmetry condition, red – runner, yellow – wall, green – inlet, blue – opening**.**

The presence of water vapour does not necessarily cause material erosion. For cavitation pitting water vapour cavity has to be in contact with the bucket surface and the condensation has to be very fast without presence of air. For numerical simulations Rossetti at al. in [9] suggested three practical conditions for cavitation pitting:

- at time t* a cavity with at least 80% of water vapour is stuck to the bucket,
- at time t*+Δt less than 20% of water vapour is in the cavity, where $\Delta t \leq 40\mu s$,
- during the condensation process less than 10% of air is in the mixture of fluids in contact with the vapour cavity.

To check these conditions for cavitation pitting we closely observed the formation and the decay of water vapour cavities at different time steps.

At the inner side of the bucket a small and thin cavity with less than 70% of water vapour was observed (see Fig. 17). The condensation was very slow. So the conditions for cavitation pitting are not fulfilled.

The second cavity of water vapour was observed at the back side of the bucket. Its development and condensation is presented in Fig. 18. Water vapour is coloured with wall distance in order to see if vapour is stuck to the bucket and how thick the vapour cavity is. Water jets and evacuating water sheets are presented with transparent magenta, so it can be seen if vapour is inside the jet or it is in contact with air. The presentation of back side cavitation on the bucket #4 started at the moment when the first amount of vapour was observed. In the first six pictures the region with vapour enlarges. At the seventh picture the condensation started at the nib of the knife and also at the middle of the cavity. At the nib of the knife the vapour is in contact with air while most of the cavity is inside the jet. In next pictures the vapour cavity is smaller and smaller and finally completely disappeared. In the last picture the cavitation started at the back side of the next bucket. The condensation at the back side is faster than at the inner side of the bucket but still too slow to fulfil the second condition for cavitation pitting, therefore no erosion of material is expected.

As already mentioned in the first part of the paper, without cavitation modelling the pressure distribution on runner buckets is not entirely correct. In regions with cavitation the values of absolute pressure should be equal to the vapour pressure, but without cavitation modelling they are significantly lower, usually negative. When negative pressure on the back side of the bucket is obtained, the value of torque is too large. When negative pressure is obtained on the inner side of the bucket, the value of torque is too small. The effect of either including cavitation modelling, or neglecting it, on the calculated torque on the shaft was similar as for the 6-jet Pelton turbine presented in section 3.3, Fig. 14. Time averaged value of torque during one cycle was for 1.99 % higher in case when cavitation was modelled.

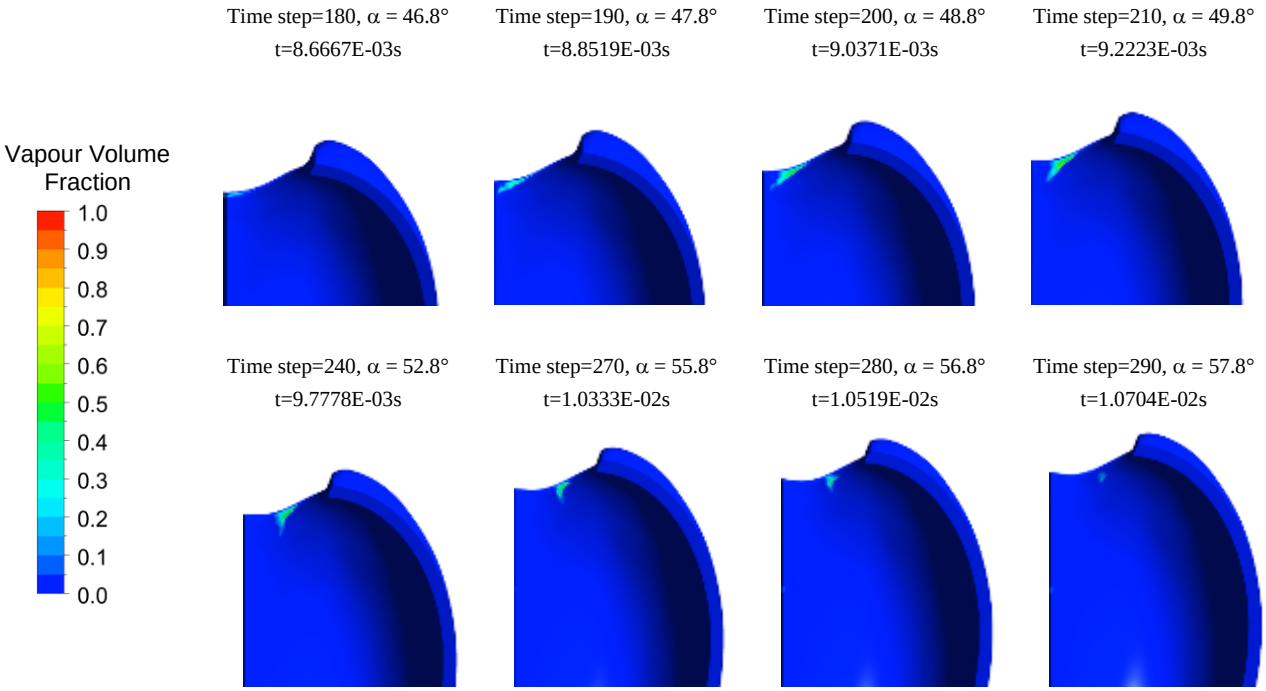

Fig. 17 Cavitation at the inner side of the bucket #4 presented with Vapour Volume Fraction

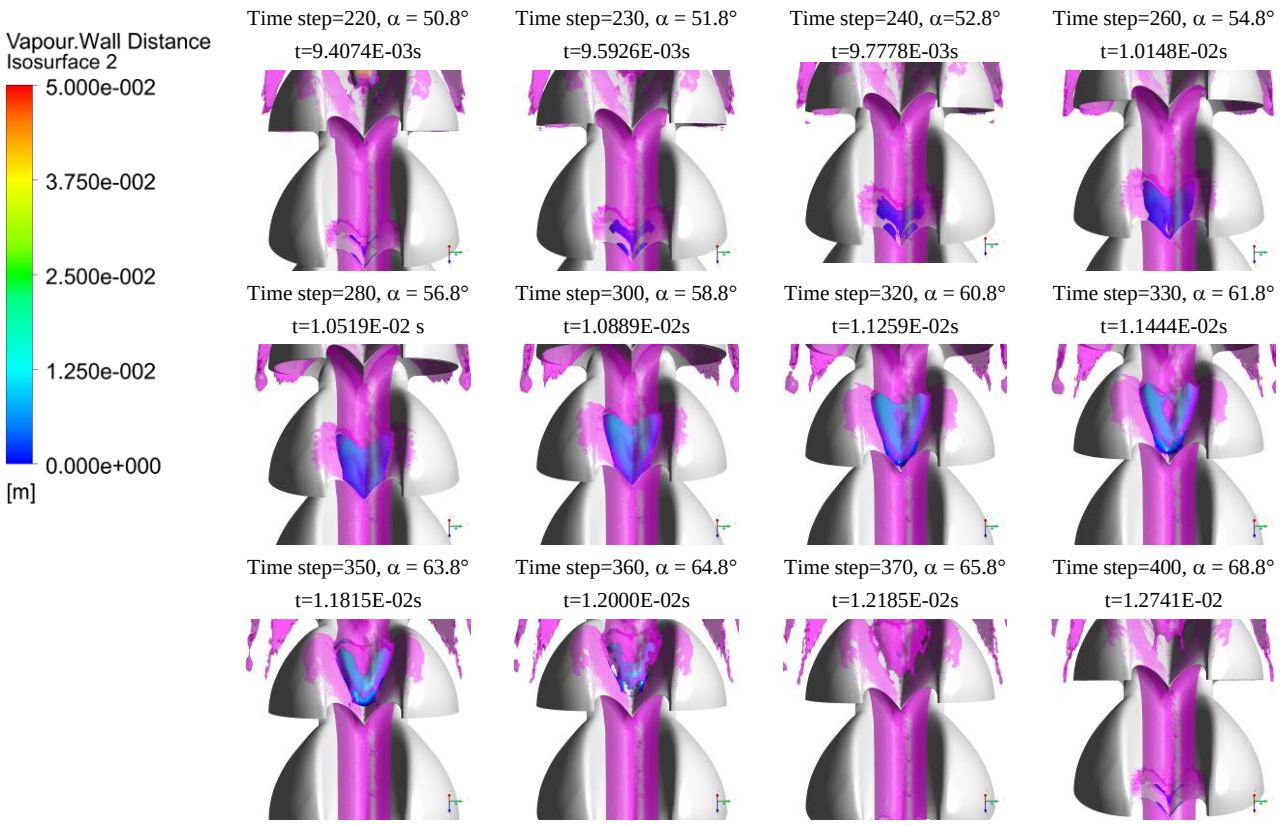

Fig. 18 Cavitation at the back side of the bucket #4.
Water is presented with iso-surface of Water Volume Fraction = 0.5 in transparent magenta.
Water vapour is presented with iso-surfaces of Vapour Volume Fraction = 0.5 coloured with Wall Distance (blue**).**

6. Conclusions

Numerical simulation can be a useful tool for qualitative and quantitative analysis of Pelton turbines. On the basis of numerical results efficiency and possible presence of cavitation can be predicted.

In this paper, a comprehensive, high-fidelity analysis of flow in Pelton turbines was considered.

In the first part of the paper the results for the model and prototype size of a 6-jet Pelton turbine are presented. From numerical results flow energy losses in the manifold and quality of the jets were obtained. From the results for 1-nozzle operation a negative correlation between secondary velocity in the jets and turbine efficiency was obtained. The effect of grid density on results was presented. Qualitative analysis of the results for the prototype size proved that there is no interaction between evacuating water sheets and the jets. As well, water evacuating from the buckets does not get in contact with the previous buckets. Numerically predicted torque on the shaft and turbine efficiency were in good agreement with the experimental values for both model and prototype size. Additional improvement of accuracy was obtained with cavitation modelling. It can be concluded that for accurate prediction of efficiency the cavitation modelling should be included in numerical simulations of Pelton runners.

In the second part of the paper the cavitation prediction for a prototype of a high head 2-jet Pelton turbine was presented. Two regions with water vapour were observed. The first one was at the inner side of the buckets near the cut-out, but the concentration of vapour was small and the condensation process was very slow. The second region with water vapour was at the back side of the bucket. Also there the condensation process was rather slow. So it can be concluded that the conditions for cavitation pitting are not fulfilled and no cavitation damages should be expected.

Acknowledgments

The research leading to these results has received funding from the People Programme (Marie Curie Actions) of the European Union's Seventh Framework Programme FP7/2007-2013/ under REA grant agreement n°612279 and from the Slovenian Research Agency ARRS - Contracts No. 1000-15-0263 and P2-0196.

Nomenclature

A_0	Relative opening [-]
$A_{0,\,BEP}$	Relative opening at BEP [-]
F_e, F_c,	Empirical coefficients [-]
H	Head [m]
M	Torque on the shaft [Nm]
Mi	Contribution of bucket #i to the torque on the shaft [Nm]
P	Pressure [Pa]
P_v	Saturation vapour pressure [Pa]
Q	Flow rate [m^3/s]
Q_i	Flow rate through nozzle #i [m^3/s]
R_B	Radius of a nucleation site [m]
S_M	Source term
$\dot{m}$	Mass transfer rate [$kg/(m^3s)$]
r_{nuc}	Nucleation site volume fraction [-]
v, U	Velocity [m/s]
v_{sec}	Secondary velocity in the jet [m/s]
ΔH	Flow energy losses [m]
ρ	Mixture density [kg/m^3]
ρ_l, ρ_v	Liquid density, vapour density [kg/m^3]
η	Turbine efficiency [-]
η_i	Turbine efficiency, active only nozzle #i [-]
η_{BEP}	Turbine efficiency at BEP [-]
η_{rel}	Relative efficiency [-], $(=\eta / \eta_{BEP})$
α	Vapour volume fraction [-]
γ	Liquid volume fraction [-]
μ	Mixture dynamic viscosity [Pa s]
μ_l	Liquid dynamic viscosity [Pa s]
μ_v	Vapour dynamic viscosity [Pa s]
τ	Stress tensor [N/m^2]

Subscripts:

Exp	experimental values

Abbreviations:

BEP	Best Efficiency Point
CFD	Computational Fluid Dynamic
SST	Shear Stress Transport
SAS	Scale Adaptive Simulation

References

[1] Parkinson, E., Garcin, H., Vullioud, G., Zhang, Z., Muggli, F. and Casartelli, E., 2002, "Experimental and numerical investigation of the free jet flow at a model nozzle of a Pelton turbine," Proceedings of the XX1st IAHR Symposium on Hydraulic Machinery and Systems, Lausanne, Switzerland.

[2] Kvicinsky, S., Kueny, J. L., Avellan, F. and Parkinson, E., 2002, "Experimental and numerical analysis of free surface flows in a rotating bucket," Proceedings of the XX1st IAHR Symposium on Hydraulic Machinery and Systems, Lausanne, Switzerland.

[3] Mack, R. and Moser, W., 2002, "Numerical investigation of the flow in a Pelton turbine," Proceedings of the XXIst IAHR Symposium on Hydraulic Machinery and Systems, Lausanne, Switzerland.

[4] Perrig, A., 2007, "Hydrodynamics of the free surface flow in Pelton turbine buckets," Ph. D. Thesis No. 3715, École polytechnique fédérale de Lausanne, Lausanne, Switzerland.

[5] Jošt, D., Mežnar, P. and Lipej, A., 2010, "Numerical prediction of Pelton turbine efficiency," IOP Conf. Ser.: Earth Environ. Sci., Vol. 12, No. 1, p. 012080, DOI: 10.1088/1755-1315/12/1/012080.

[6] Santolin, A., Cavazzini, G., Ardizzon, G. and Pavesi, G., 2009, "Numerical investigation of the interaction between jet and bucket in a Pelton turbine," Proc. Inst. of Mech. Engineers Part A, J. Power Energy, Vol. 223, No. 6, pp. 721-728.

[7] Marongiu, J., Leboeuf, F., Caro, J. and Parkinson, E., 2010, "Free surface flows simulations in Pelton turbines using a hybrid SPH-ALE Method," J. Hydraulic Res., Vol. 48, No. sup1, pp. 40-49, DOI: 10.1080/00221686.2010.9641244.

[8] Vessaz, C., Jahanbaksh, E. and Avellan, F., 2015, "Flow simulation of jet deviation by rotating Pelton buckets using finite volume particle method," J. Fluids Eng., Vol. 137, No. 7, p. 074501.

[9] Rosetti, A., Pavesi, G., Ardizzon, G. and Santolin, A., 2014, "Numerical analyses of cavitating flow in a Pelton turbine," J. Fluids Eng., Vol. 136, No. 8, p. 081304.

[10] Jošt, D., Škerlavaj, A., Pirnat, V., Morgut, M., Nobile, E., 2018, "Numerical prediction of efficiency and cavitation for a Pelton turbine," IOP Conf. Ser.: Earth Environ. Sci., Vol. 240, No. 6, p. 062033, DOI: 10.1088/1755-1315/240/6/062033.

[11] Zwart, P. J., Gerber, A. G. and Belamri, T., 2004, "A two-phase model for predicting cavitation dynamics," Fifth International Conference on Multiphase Flow, Yokohama, Japan.

[12] Morgut, M., Jošt, D., Škerlavaj, A., Nobile, E., Contento, G., 2018, "Numerical Predictions of Cavitating Flow Around a Marine Propeller and Kaplan Turbine Runner with Calibrated Mass Transfer Models," Strojniški Vestnik – Journal of Mechanical Engineering, Vol. 64, No. 9, pp. 543-554, DOI:10.5545/sv-jme.2017.4647.

[13] Menter, F., 1994, "Two-equation eddy-viscosity turbulence models for engineering applications," AIAA Journal, Vol. 32, No. 8, pp. 1598-1605, DOI:10.2514/3.12149.

[14] Egorov, Y., and Menter. F., 2007, "Development and Application of SST-SAS Turbulence Model in the DESIDER Project," Proc. Second Symposium on Hybrid RANS-LES Methods, Corfu, Greece.

[15] ANSYS, 2013, CFX Solver Theory Guide, Release 15.0.

[16] Staubli, T., Abgottspon, A., Weibel, P., Bissel, C., Parkinson, E., Leduc, J. and Leboeuf, F., 2009, "Jet quality and Pelton efficiency," Hydro 2009, Lyon, France.